Z. Phys. D – Atoms, Molecules and Clusters 21, 163–175 (1991)

Atoms, Molecules
Zeitschrift für Physik D and Clusters

Shell-structure and octupole instability in fermion systems

I. Hamamoto, B. Mottelson[1], H. Xie, and X.Z. Zhang*

Department of Mathematical Physics, University of Lund, Lund, Sweden
[1] NORDITA, Copenhagen, Denmark

Received 19 January 1991

Abstract. Simulating the one-particle spectra of the infinite-well potential by a model, we study the symmetry and the shell-structure of octupole deformations as well as the possible occurrence of octupole (and quadrupole) instabilities. Among various types of octupole deformations investigated the Y_{32}-type deformation is found to have a strong shell-structure as well as a very interesting symmetry which leads to the occurrence of highly-degenerate single-particle levels. One particle spectra of the octupole-coupled two-level model (with ℓ and $\ell+3$) are analytically studied in the limit of large angular-momentum, ℓ.

PACS: 03.65.; 36.40.+d; 21.60.−n

1. Introduction

The occurrence of spontaneous symmetry breaking leading to shapes with a variety of symmetries has been discussed for atomic nuclei; the majority of the observed shapes are of spheroidal form but the possibility of octupole deformation has also been a topic of recurring interest [1]. Only the Y_{30}-deformation has so far been theoretically studied in the nuclear physics literature, though there seems to be no obvious reason to ignore the possible occurrence of other types of octupole deformations such as Y_{31}, Y_{32} or Y_{33} deformations. In [2] a possible octupole instability for configurations with many particles outside of closed shells is discussed in terms of the periodic classical orbits characterizing the shell-structure. Though the discussion in [2] indicates an approach to octupole instability in heavier nuclei (beyond ^{208}Pb), even the heaviest nuclear system (for example, the neutron number, $N \sim 150$) seems to have a bit too small number of particles to realize large octupole deformations in its ground state as a result of the shell-structure. The discussion in [2] shows that an octupole instability might be realized for a system with a smaller number of particles, if the one-particle potential has a more sharply defined surface than for the nuclear potential.

The study of clusters of metalic atoms has revealed the existence of shell structure based on single particle motion of electrons [3] and evidence has been provided for the concomitant occurrence of deformations. These studies open the possibility of exploring deformation effects at much higher quantum numbers than observed in the nuclear systems and in particular octupole deformations may be expected to play an important role.

In Fig. 1 the one-particle spectrum in the spherically-symmetric infinite square-well potential is plotted as a function of the orbital angular-momentum of particles. It is seen that the energies of the lowest $\ell=7$ state and the second-lowest $\ell=4$ state are nearly degenerate and are relatively separated from the energies of other states.

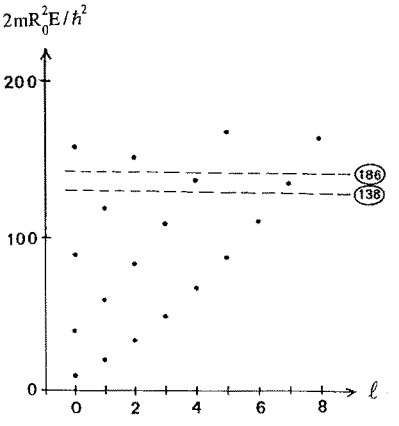

Fig. 1. One-particle spectrum for spherically-symmetric infinite square-well potential. The orbital angular-momentum of particles is expressed by ℓ, while R_0 denotes the radius of the sphere. Some particle-numbers, which are obtained by filling the orbitals up to a given level including the spin ($=1/2$) degree of freedom, are indicated with a circle

* *Permanent address:* Institute of Atomic Energy, Beijing, The People's Republic of China

The near degeneracy of a pair of orbits with ℓ and $\ell+3$ may suggest a possibility of gaining energy by octupole-deforming the system. Counting from the bottom including the spin ($=1/2$) degree of freedom, the filling of those two orbitals (with $\ell=7$ and $\ell=4$) corresponds to a system with the particle-number, $138<N\leqq 186$. In most of the numerical examples in the present paper we discuss this major shell with the particle-number, $138<N\leqq 186$.

In Sect. 2 both the symmetry of the octupole deformations as well as the bunching of the one-particle spectra in the octupole-deformed field is discussed, taking an example in which the two levels with the angular-momentum ℓ and $(\ell+3)$ are degenerate in the limit of spherically-symmetric shape. In Sect. 3 the octupole-instability of the system with "an infinite square-well potential", which is simulated by a modified oscillator potential, is investigated. The quadrupole-instability of the same system as the one used in Sect. 3 is examined in Sect. 4, and the possibility of the octupole deformation is compared with that of the quadrupole deformation. Conclusions are discussed in Sect. 5. In Appendix A the symmetry structure of octupole deformations is clarified in terms of group theory. In Appendix B we present the calculated result of axially-symmetric quadrupole deformation of the exact infinite-square-well potential, using the method in which the volume-conservation is exactly taken into account. In Appendix C the structure of the one-particle spectrum of the two-level model described in Sect. 2 is analytically studied in detail in the limit of large angular-momentum.

2. Octupole-deformation and two-level model

Deformation with octupole symmetry can be characterized by a set of $7(=(2\lambda+1)$ where $\lambda=3)$ amplitudes, considering the Hermitian property of the Hamiltonian. Without going into the discussion of the definition of the Euler angles to define the orientation of an intrinsic coordinate system, in the present article we consider four separate amplitudes corresponding to the following types of the deformation,

$$Y_{30},(Y_{31}-Y_{3-1}),(Y_{32}+Y_{3-2}),\quad\text{and}\quad(Y_{33}-Y_{3-3}).\qquad(1)$$

As far as we take into account only one of the above four deformations at a time, the deformations of the other combinations of $Y_{3\nu}$, namely $(Y_{31}+Y_{3-1})$, $(Y_{32}-Y_{3-2})$ and $(Y_{33}+Y_{3-3})$, give rise to the same shape as $(Y_{31}-Y_{3-1})$, $(Y_{32}+Y_{3-2})$ and $(Y_{33}-Y_{3-3})$, respectively.

First, we consider a simplified case in which two orbitals with ℓ and $(\ell+3)$ are octupole-coupled. In Fig. 2 we show the result of the diagonalization taking into account one type of the deformations in (1) at a time, when in the spherically-symmetric limit the two states with $\ell=4$ and $\ell=7$ are exactly degenerate. The degeneracy of the resulting levels (before including the spin degree of freedom) is shown in the figure. (Note that in the spherical limit the degeneracy is 24 $(=2\times4+1+2\times7+1)$ fold.) In the octupole coupling of

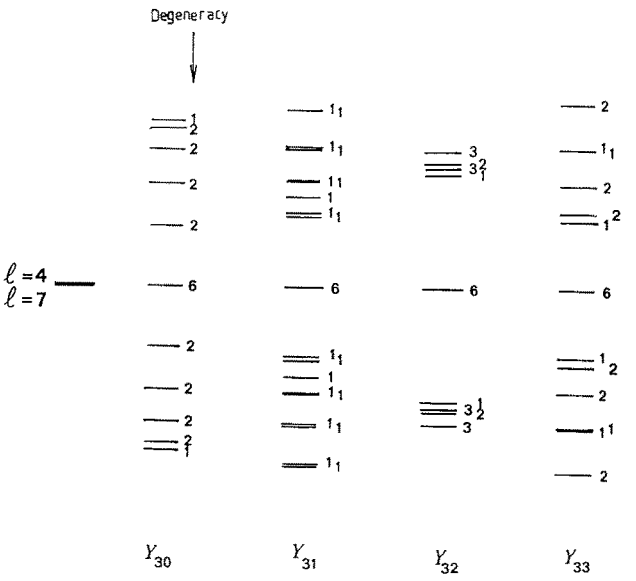

Fig. 2. One-particle spectra obtained by taking into account one type of octupole couplings in (1) at a time, in the case that the two states with $\ell=4$ and $\ell=7$ are exactly degenerate in the spherically symmetric limit. The degeneracy of the resulting levels (without including the spin degree of freedom) is shown in the figure. The relative magnitude between the level-splittings for different type of octupole couplings has no special meaning

the degenerate ℓ and $\ell+3$ states there are always 6 levels which have energies unaffected by the coupling. In Fig. 2 we note two kinds of shell-structure which depend on the type of the octupole deformation: (*a*) the degree of the degeneracy of the resulting levels; (*b*) the feature of the level-bunching.

On (*a*): For the Y_{30}-deformation the system is axially-symmetric and the z-component of the angular-momentum, m, is a good quantum-number. The $m=0$ level is singly-degenerate, while the $m\neq0$ levels are doubly-degenerate with positive and negative m-values. For the Y_{31}-deformation there is no degeneracy, before the spin degree of freedom is taken into account. For the Y_{32}-deformation there are, in general, triply-, doubly- and singly-degenerate levels. This can be easily understood because the deformation of the type, $(Y_{32}+Y_{3-2})$, has the symmetry of the T_d-group [4], consisting of all the symmetry transformations of the tetrahedron. For the Y_{33}-deformation there are doubly- and singly-degenerate levels. This is understood since the deformation of the type, $(Y_{33}-Y_{3-3})$, has the symmetry of the D_{3h}-group. In Appendix A we clarify the degeneracy of the bunched levels in the presence of octupole deformations using the irreducible representations of the groups, in which respective deformations are invariant.

On (*b*): For the $(Y_{32}+Y_{3-2})$ deformation we observe a very prominent bunching of the resulting levels, compared with other types of octupole deformations. This feature of the bunching is going to play a crucial role also when we estimate the shell-structure energy for a more realistic model (see Sect. 3).

The above observations (*a*) and (*b*) are general features of the one-particle spectra in octupole deforma-

tions, though the presence of the uncoupled 6 levels in Fig. 2 is a special feature in the degenerate two-level (with ℓ and $\ell+3$) model. The patterns observed in Fig. 2 are further illuminated by the study of the asymptotic solution ($\ell \gg 1$) of the two-level model as discussed in Appendix C.

3. Octupole deformation in infinite square-well potential – simulation by model calculation

By using a modified oscillator model which has been extensively employed in nuclear physics [2, 5] for many years, we simulate the single-particle energy spectrum in an infinite square-well potential. However, for quadrupole deformations a simple and accurate technique for obtaining the energy spectrum in an exact infinite square-well potential is known [6]. In Appendix B we compare the calculated result obtained from this technique with ours, partly in order to check the effect of our approximate-treatment of the volume-conservation condition on our conclusion.

Our potential is written as

$$V(\mathbf{r})=\frac{1}{2}m\omega_0^2 r^2\left\{1+\varepsilon_{30}\,Y_{30}+\frac{\varepsilon_{31}}{\sqrt{2}}(Y_{31}-Y_{3-1})+\frac{\varepsilon_{32}}{\sqrt{2}}(Y_{32}+Y_{3-2})+\frac{\varepsilon_{33}}{\sqrt{2}}(Y_{33}-Y_{3-3})\right\}+v_{\ell\ell}\hbar\omega_0(\vec{\ell}^2-\langle\vec{\ell}^2\rangle_N), \tag{2}$$

where

$$\langle\vec{\ell}^2\rangle_N=\tfrac{1}{2}N(N+3). \tag{3}$$

In the case that all $\varepsilon_{3\nu}$ vanish the potential corresponds to a spherical harmonic oscillator with the addition of a term proportional to $\vec{\ell}^2$. The latter lifts the degeneracy within each major oscillator shell in such a way as to lower the states with large ℓ, resulting in a level-ordering corresponding to a potential with a more sharply-defined surface. The values of the constants $v_{\ell\ell}$, which simulate the spectrum in the infinite square-well potential, are taken from Fig. 6-49 of [2]. In Fig. 3 we show the calculated single-particle spectrum for the case of all $\varepsilon_{3\nu}=0$, which should be compared with the spectrum in Fig. 1. Note that the energy units used are different in Fig. 3 from those in Fig. 1. Namely, $\hbar\omega_0 \sim N^{-1/3}$ for a saturated system with the particle-number N, while $R_0^{-2} \sim N^{-2/3}$ in Fig. 1. Nevertheless, we can duly compare the level-order as well as the near-degeneracy of the levels in the two figures. We notice that the main structure of the spectrum in Fig. 1, especially the near-degeneracy of the $\ell=4$ and $\ell=7$ states, is well reproduced by using the $\vec{\ell}^2$-term in (2). In the following numerical calculations we take the modified oscillator potential, (2), and not the exact infinite square-well potential. (However, see Appendix B.)

In Figs. 4, 5, 6, 7 and 8 we show examples of the calculated single-particle spectra ("the Nilsson diagram" in the nuclear physics [5]) for the octupole-deformations including only one type of the deformation at a time (i.e. only one of $\varepsilon_{3\nu}$ is non-vanishing at a time). In the calculation all the harmonic oscillator bases with $N \leqq 14$ are included. The particle-numbers, which are obtained by filling in all the lower-lying levels from the bottom including the spin ($=1/2$) degree of freedom, are shown in several places of the figures. Because of the spin degree of freedom, all levels are at least doubly-degenerate (i.e.

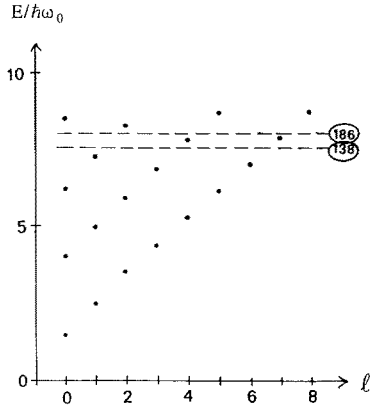

Fig. 3. One-particle spectrum for our spherically-symmetric modified-oscillator potential, which simulates the spectrum for infinite-square-well potential. The orbital angular-momentum of particles is denoted by ℓ. Some particle-numbers, which are obtained by filling the orbitals up to a given level including the spin degree of freedom, are indicated with a circle. Note the difference between the used energy-unit in Fig. 1 and that in Fig. 3

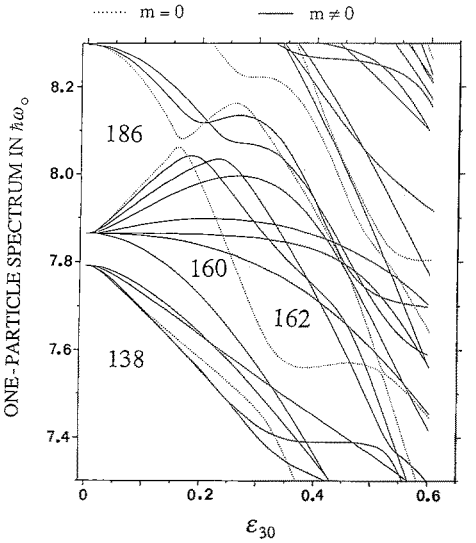

Fig. 4. One-particle spectra calculated for the octupole-deformation of the type Y_{30}. Octupole-deformation amplitudes $\varepsilon_{3\nu}$ other than $\nu=0$ are set equal to zero. In the numerical calculations the right-hand-side quantity in (3) is replaced by $\frac{1}{2}(N+\frac{3}{2})^2$. The consequence of the replacement is a small nearly-constant shift of the energy in the figure and, thus, has no physical significance. Some particle-numbers, which are obtained by filling the orbits up to a given level including the spin ($=1/2$) degree of freedom, are indicated in the figure. The lower-lying level between the particle-number 138 and 186 at $\varepsilon_{30}=0$ is the second-lowest $\ell=4$ state, while the higher-lying level is the lowest $\ell=7$ state. The $m=0$ orbitals drawn by dotted lines accommodate 2 particles, while the $m\neq 0$ orbitals indicated by solid lines can be filled in by 4 particles

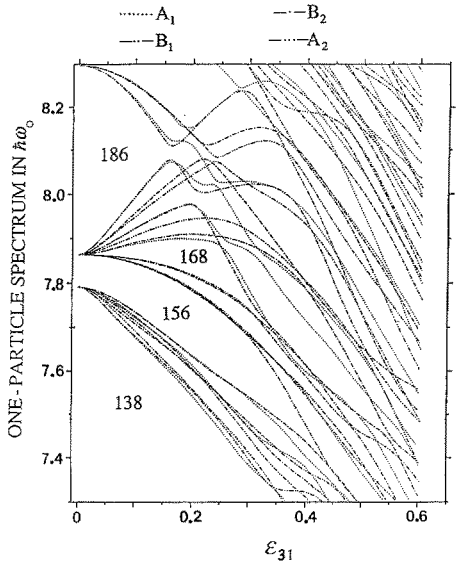

Fig. 5. One-particle spectra calculated for the octupole-deformation of the type $(Y_{31}-Y_{3-1})$. Octupole-deformation amplitudes ε_{3v} other than $v=1$ are set equal to zero. The irreducible representations of the C_{2v} group are expressed by A_1, A_2, B_1 and B_2, all of which are one-dimensional representations and, thus, can accommodate 2 particles. See the caption to Fig. 4

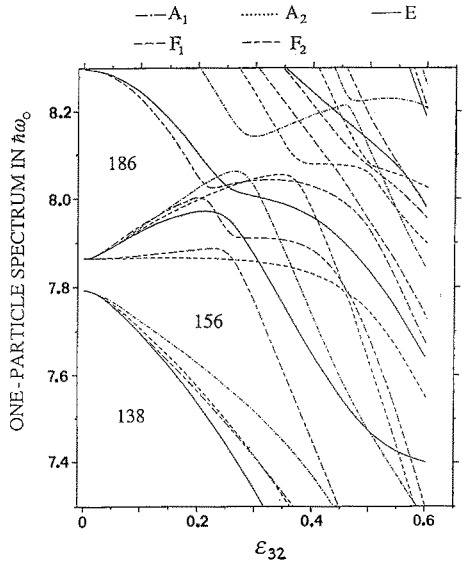

Fig. 6. One-particle spectra calculated for the octupole-deformation of the type $(Y_{32}+Y_{3-2})$. Octupole-deformation amplitudes ε_{3v} other than $v=2$ are set equal to zero. The irreducible representations of the T_d group are denoted by A_1(1-dim.), A_2(1-dim.), E(2-dim.), F_1(3-dim.) and F_2(3-dim.), which can accommodate 2, 2, 4, 6 and 6 particles, respectively. See the caption to Fig. 4

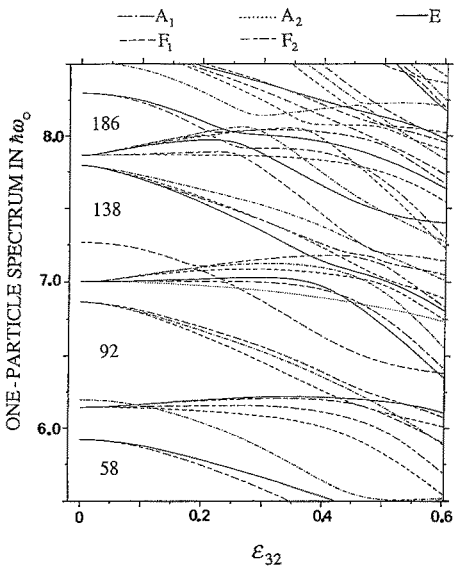

Fig. 7. One-particle spectra calculated for the octupole-deformation of the type $(Y_{32}+Y_{3-2})$, for a larger region of the particle number than that shown in Fig. 6. See the text and the caption to Fig. 6

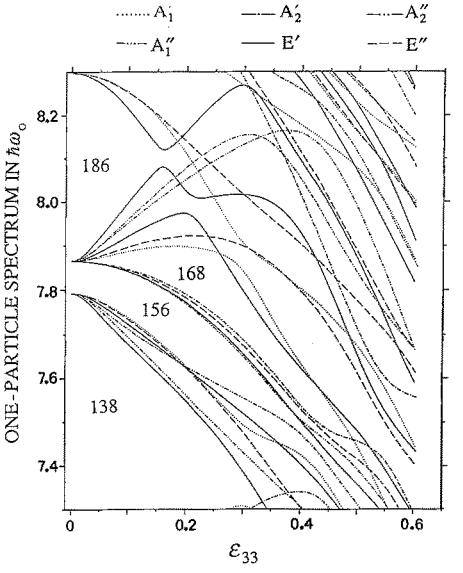

Fig. 8. One-particle spectra calculated for the octupole-deformation of the type $(Y_{33}-Y_{3-3})$. Octupole-deformation amplitudes ε_{3v} other than $v=3$ are set equal to zero. The irreducible representations of the D_{3h} group are denoted by A_1'(1-dim.), A_2'(1-dim.), A_1''(1-dim.), A_2''(1-dim.), E'(2-dim.) and E''(2-dim.), which can accommodate 2, 2, 2, 2, 4 and 4 particles, respectively. See the caption to Fig. 4

spin-up and spin-down). In Fig. 4 for the Y_{30}-deformation the $m=0$ ($m\neq 0$) levels can accommodate 2 (4) particles. In Fig. 5 for the Y_{31}-deformation one-particle levels are classified in terms of the irreducible representations (A_1, A_2, B_1, B_2) of the C_{2v} group. The interaction can only exist between the one-particle levels belonging to the same irreducible representation. All the irreducible representations are one-dimensional and, thus, can accommodate 2 particles when the spin degeee of freedom is included. In Fig. 6 for the Y_{32} deformation one-particle levels are classified in terms of the irreducible representations (A_1, A_2, E, F_1, F_2) of the T_d group. Including the spin degree of freedom one can fill 2, 4, and 6 particles in A_1 and A_2, E, F_1 and F_2, respectively. Since the A_2 representation is not seen in Fig. 6, we show Fig. 7 which covers a larger region of the one-particle spectrum. In Fig. 7 the orbital belonging to the A_2 representation is seen originating from the $\ell=6$ orbi-

tal in the spherically-symmetric limit, of which the energy is about (7.0) $\hbar\omega_0$. In Fig. 8 for the Y_{33} deformation one-particle levels are classified in terms of the irreducible representations (A_1', A_2', A_1'', A_2'', E', E'') of the D_{3h} group. The A representations can accommodate 2 particles counting the spin degree of freedom, while the E representations accommodate 4 particles.

Due to the near-degeneracy of the $\ell=7$ and $\ell=4$ states in the spherical limit, for smaller deformations in Figs. 4, 5, 6, 7 and 8 we observe a structure of the bunching (or the splitting) of levels which is very similar to those shown in Fig. 2. For larger deformations the presence of levels lying far away in the spherical limit starts to affect the bunching of the levels. It is a general feature that the Y_{32}-deformation produces by far the most prominent bunching of the levels compared with other types of octupole deformations. From Fig. 6 it is observed that the particle-number $N=156$, for example, exhibits a kind of shell-closure for a moderate size of the Y_{32}-deformation. The energy unit, $\hbar\omega_0$, used in Figs. 4–8 has, in general, a dependence on the size of deformations. Thus, from the figures one cannot directly read the deformation of the energy-minimum for a given particle-number.

Next, we require a constant volume of the system when it is deformed, in order to specify the deformation-dependence of ω_0. Neglecting the contribution from the $\vec{\ell}^2$ term to the volume conservation, we obtain [5] from the potential in (2)

$$\frac{\omega_0^3}{\mathring{\omega}_0^3}=\frac{1}{4\pi}\int\!\!\int \frac{\sin\theta\,\mathrm{d}\theta\,\mathrm{d}\varphi}{[1+\varepsilon_{30}\,Y_{30}+\frac{\varepsilon_{31}}{\sqrt{2}}(Y_{31}-Y_{3-1})+\frac{\varepsilon_{32}}{\sqrt{2}}(Y_{32}+Y_{3-2})+\frac{\varepsilon_{33}}{\sqrt{2}}(Y_{33}-Y_{3-3})]^{3/2}}, \tag{4}$$

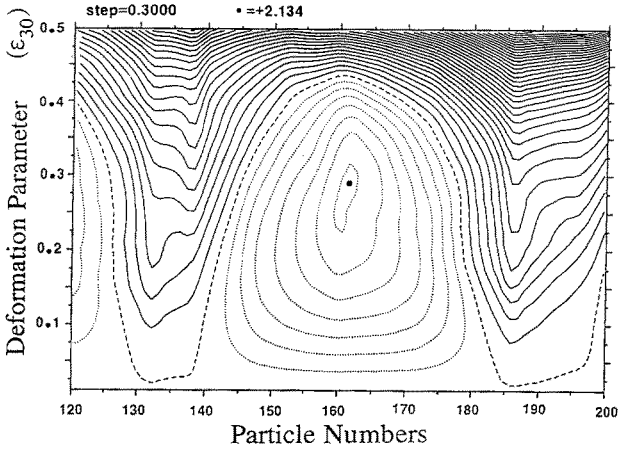

Fig. 9. The contour map of the quantity defined in (5), in which all $\varepsilon_{3\nu}$-values except $\nu=0$ are set equal to zero. The dotted line (the solid line) shows a positive (negative) sign of the quantity (5), while the dashed line corresponds to vanishing of the quantity (5). A step between the lines is $(0.30)\hbar\mathring{\omega}_0$, where $\mathring{\omega}_0$ is independent of deformations. For a given particle-number the dotted line area is energetically more favoured than the spherical shape. The quantity (5) reaches the maximum value ($=2.13\hbar\mathring{\omega}_0$) at $\varepsilon_{30}=0.29$ for the system $N=162$

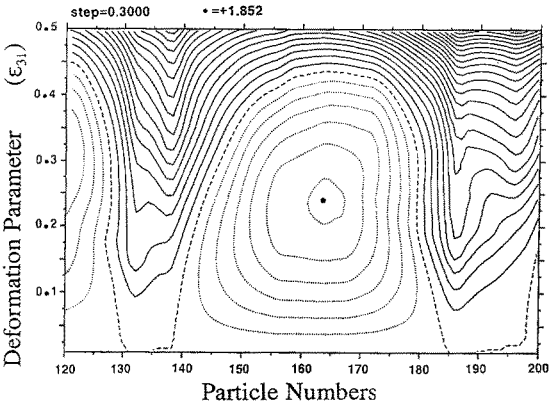

Fig. 10. The contour map of the quantity (5), in which all $\varepsilon_{3\nu}$-values except $\nu=1$ are set equal to zero. See the caption to Fig. 9. The quantity (5) reaches the maximum value ($=1.85\hbar\mathring{\omega}_0$) at $\varepsilon_{31}=0.23$ for the system with $N=164$

where $\mathring{\omega}_0$ is the value of ω_0 in the spherical limit. In Figs. 9–12 we plot the contour map of the quantities

$$\sum_{i=1}^{N} e_i(\varepsilon_{3\nu}=0)-\sum_{i=1}^{N} e_i(\varepsilon_{3\nu}) \tag{5}$$

expressed in units of $\hbar\mathring{\omega}_0$ as a function of both the deformation-parameters and the particle-number N (for $120\leqq N\leqq 200$). In the expression (5) $e_i(\varepsilon_{3\nu})$ denotes the i-th one-particle energy for the deformation amplitude $\varepsilon_{3\nu}$. For a given particle-number N the first term in (5) is constant and, thus, the $\varepsilon_{3\nu}$-value at the maximum of the expression (5) gives the deformation at the energy minimum. In other words, the quantity (5) expresses the gain of the summed energy by deforming the system with $\varepsilon_{3\nu}$. The sum appearing in (5) is not really equal to the total energy of the system, but is, for example, equal to 4/3 of the total energy in the limit of the harmonic oscillator, assuming that the potential comes from the two-body interaction. In the following we neglect the dfference between the sums in (5) and the total energy, since we look for the deformation at the energy-minimum and we never discuss the absolute magnitude of the total energy.

In Figs. 9–12 the dotted-line shows a positive sign of the quantity (5) (namely, for a given particle-number the dotted line area is energetically more favourable than the spherical shape), the dashed-line corresponds to a vanishing quantity (5), while the solid line expresses a

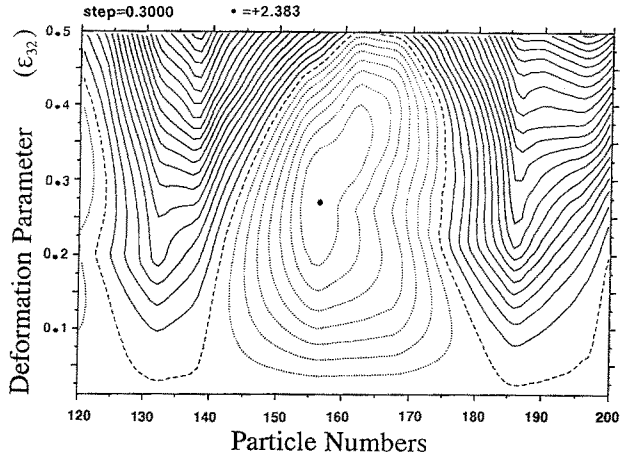

Fig. 11. The contour map of the quantity (5), in which all ε_{3v}-values except $v=2$ are set equal to zero. See the caption to Fig. 9. The quantity (5) reaches the maximum value ($=2.38\hbar\mathring{\omega}_0$) at $\varepsilon_{32}=0.27$ for the system with $N=156$

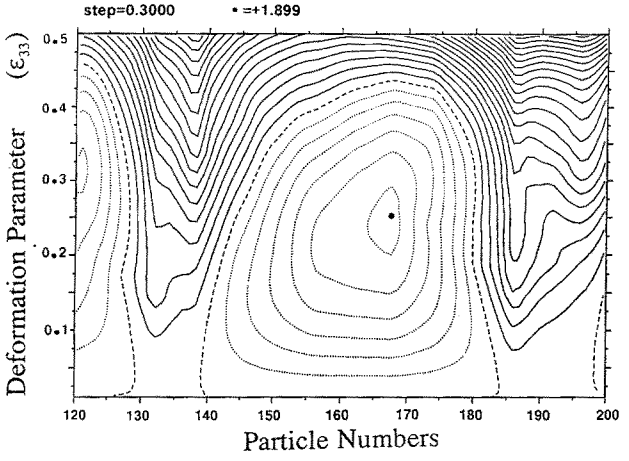

Fig. 12. The contour map of the quantity (5), in which all ε_{3v}-values except $v=3$ are set equal to zero. See the caption to Fig. 9. The quantity (5) reaches the maximum value ($=1.90\hbar\mathring{\omega}_0$) at $\varepsilon_{33}=0.26$ for the system with $N=168$

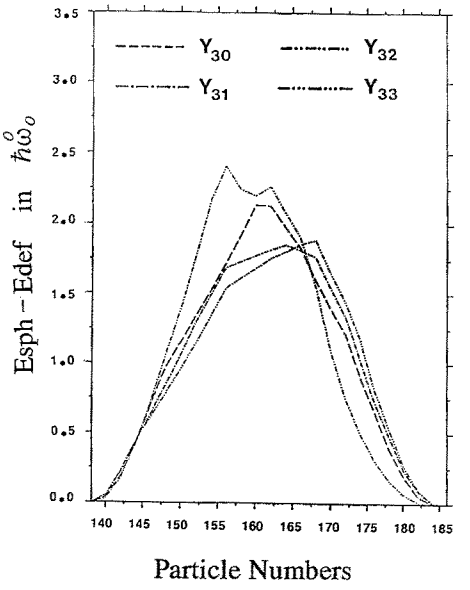

Fig. 13. The quantity (5) calculated at the ε_{3v}-value, which is energetically most favourable for each type of v at given particle-numbers

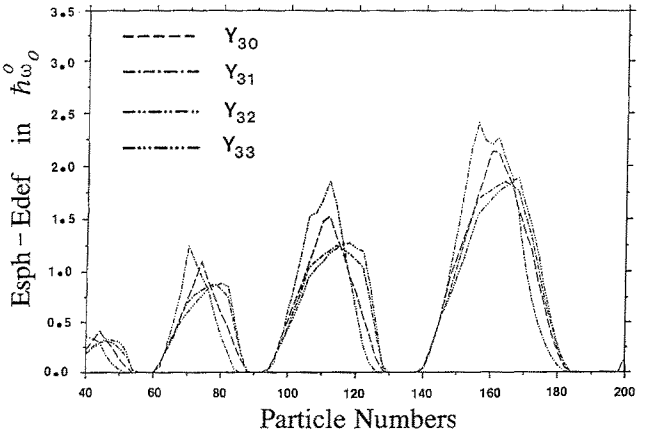

Fig. 14. The same quantity as in Fig. 13, but for a larger region of the particle-number

negative sign of (5). The step between the lines is $(0.30)\hbar\mathring{\omega}_0$. For example, from Fig. 11 we see that the quantity (5) reaches the maximum value ($=(2.38)\hbar\mathring{\omega}_0$) at $\varepsilon_{32}=0.27$ for the system with $N=156$. Note that the quantity (5), which is plotted in Figs. 9–12, is different from the socalled potential-energy surface in the Strutinsky-type calculations, in which the subtracted quantity is either the smeared out sum of one-particle energies or the liquid-drop energies and not the sum of one-particle energies for spherical shape.

In Fig. 13 the maximum of the quantity in (5) for a given particle-number which can be obtained from Figs. 9–12 is plotted for the respective type of deformation. In this way we see which type of the self-consistent deformations is energetically most favourable for a given particle-number. It is seen that for a few particles added to the spherical "closed shell" with $N=138$ the Y_{33}-deformation is most favourable; for more particles outside of the $N=138$ closed-shell the Y_{32}-deformation is by far the most favourable; for the particle-number $N\geqq 168$ the Y_{33}-deformation is again most favourable. It is interesting to observe that for any particle-number, the axially-symmetric octupole deformation (i.e. the Y_{30}-deformation) in its self-consistent magnitude never becomes most favourable.

In Fig. 14 we show the same quantity as given in Fig. 13 for a larger region of particle-numbers.

4. Octupole deformation versus quadrupole deformation

In the examples discussed in the previous Sects. 2 and 3 there is always a possibility of gaining energy by quadrupole-deforming the system from a spherical shape, instead of octupole-deforming the system. Then, an interesting question is whether the most favourable octupole deformation can be energetically lower than the most favourable quadrupole deformation or not.

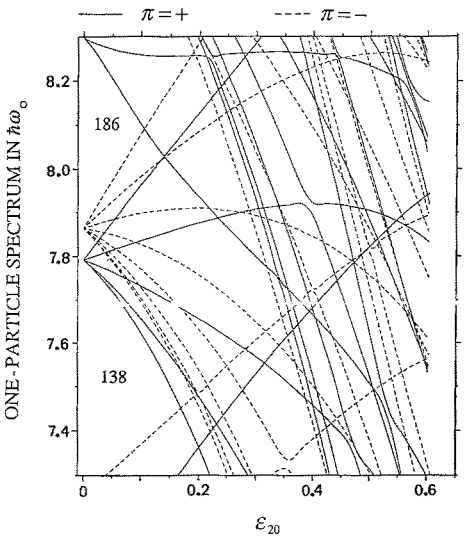

Fig. 15. One-particle spectra for the axially-symmetric quadrupole deformation of prolate shape (i.e. $\varepsilon_{20}>0$). Namely, in the expression (6) we set $\varepsilon_{22}=0$ and use the same $v_{\ell\ell}$-values as those used for octupole deformations in Sect. 3. Some particle-numbers, which are obtained by filling the orbitals up to a given level including the spin ($=1/2$) degree of freedom, are indicated in the figure. The positive-parity ($\pi=+$) orbitals are drawn by solid lines, while the negative-parity ($\pi=-$) orbitals are expressed by dashed lines

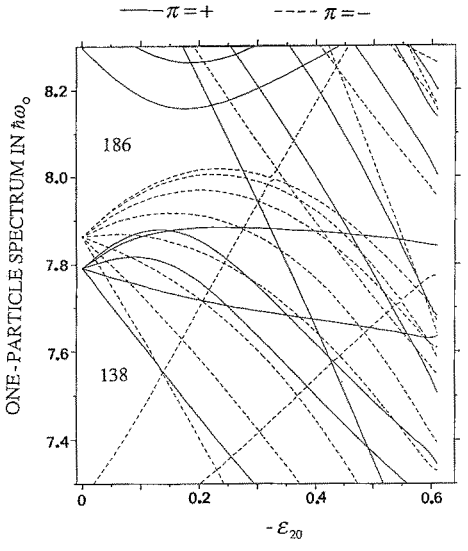

Fig. 16. One-particle spectra for the axially-symmetric quadrupole deformation of oblate shape (i.e. $\varepsilon_{20}<0$). See the caption to Fig. 15

Using the quadrupole-deformed modified oscillator potential

$$V(\mathbf{r})=\frac{1}{2}m\omega_0^2 r^2\left\{1+\varepsilon_{20}\,Y_{20}+\frac{\varepsilon_{22}}{\sqrt{2}}(Y_{22}+Y_{2-2})\right\}+v_{\ell\ell}\,\hbar\omega_0(\vec{\ell}^2-\langle\vec{\ell}^2\rangle_N), \tag{6}$$

where the constants $v_{\ell\ell}$ are the same as those used in Sect. 3, we repeat the calculation described in Sect. 3. In Figs. 15 and 16 we show the "Nilsson diagram" for axially-symmetric quadrupole deformations, prolate shape and oblate shape, respectively. A prolate (oblate)

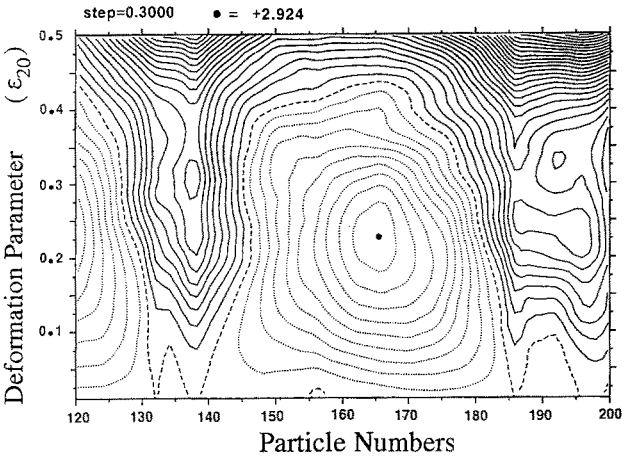

Fig. 17. The contour map of the quantity in (5), in which ε_{3v} is replaced by $\varepsilon_{20}>0$. See the caption to Fig. 9. The quantity (5) reaches the maximum value ($=2.92\hbar\hat{\omega}_0$) at $\varepsilon_{20}=0.22$ for the system with $N=166$

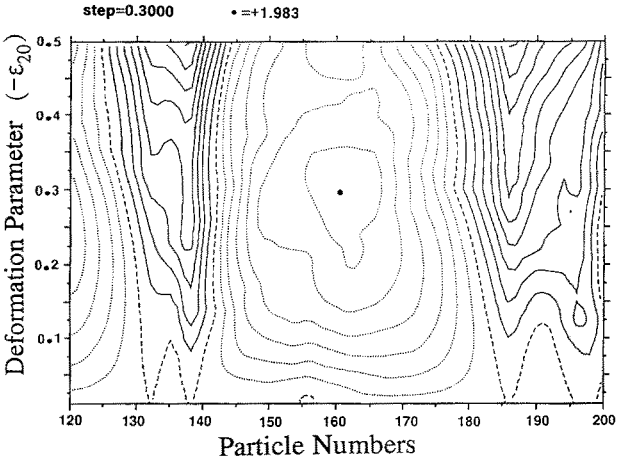

Fig. 18. The contour map of the quantity in (5), in which ε_{3v} is replaced by $\varepsilon_{20}<0$. See the caption to Fig. 9. The quantity (5) reaches the maximum value ($=1.98\hbar\hat{\omega}_0$) at $\varepsilon_{20}=-0.30$ for the system with $N=160$

shape corresponds to the parameter-region with $\varepsilon_{20}>0(\varepsilon_{20}<0)$ and $\varepsilon_{22}=0$. Taking into account the volume-conservation condition in a similar way to the one in (4), in Figs. 17 and 18 we show the contour map of the quantities in (5), in which ε_{3v} is replaced by ε_{2v}, for prolate shape and oblate shape, respectively.

In Fig. 19 the maximum of the quantity in (5), in which ε_{3v} is replaced by ε_{2v}, for a given particle-number is plotted for $\varepsilon_{20}>0$ (prolate), $\varepsilon_{20}<0$ (oblate) and general triaxial shapes, respectively. From Fig. 19 it is seen that at the beginning of the major shell (with $138<N\leqq 186$) almost oblate shapes are most favourable, while at the second half of the shell almost prolate shapes are most favourable. By "almost" oblate (or prolate) shape we mean that the shape at the energy-minimum may have a deviation from the axially-symmetric deformation, depending on the particle-number. However, except for the region of the particle-number, $152<N<158$, the deviation is very small and the energy gain by the deviation

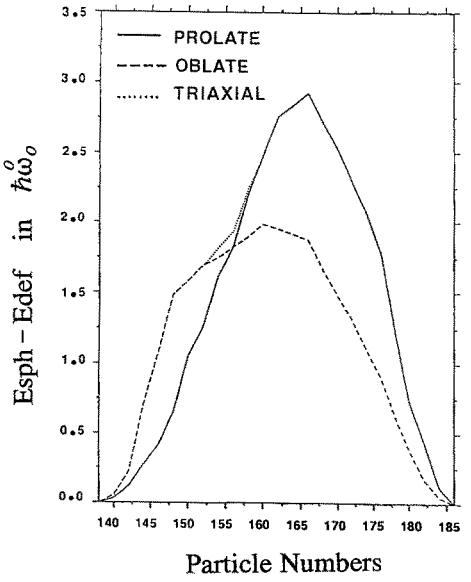

Fig. 19. The maximum of the quantity in (5), in which ε_{3v} is replaced by ε_{2v}, for given particle-numbers. The solid line corresponds to prolate shape (i.e. $\varepsilon_{20}>0$ and $\varepsilon_{22}=0$), and the dashed line to oblate shape (i.e. $\varepsilon_{20}<0$, $\varepsilon_{22}=0$), while the dotted line corresponds to energetically most favourable triaxial shape (i.e. $\varepsilon_{22}\neq 0$)

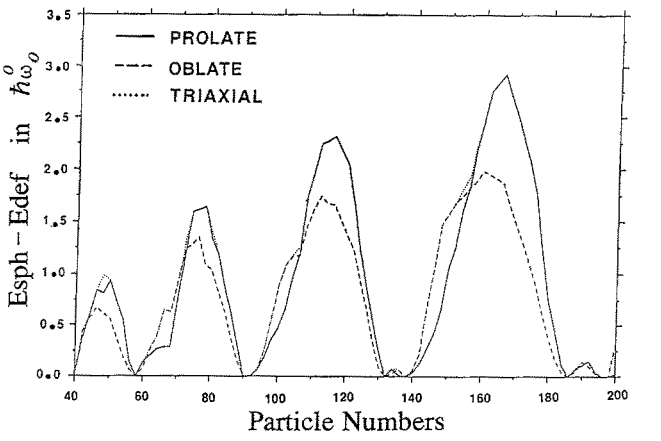

Fig. 20. The same quantity as Fig. 19, but for a larger region of the particle-number

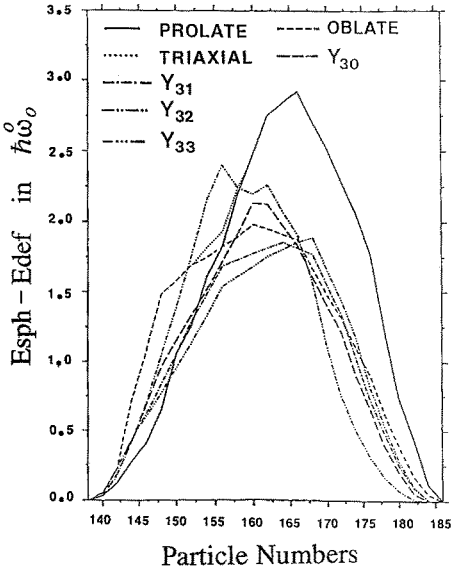

Fig. 21. Plotting of Fig. 13 (for octupole deformations) and Fig. 19 (for quadrupole deformations) in the same frame

is almost negligibly small. This preference of oblate or prolate shape depending on the degree of major-shell filling is a feature of a single-ℓ-shell and is opposite to the case of a harmonic oscillator potential or the case of the observed deformation of the nuclear one-body potential. In the latter two cases prolate shapes are favourable at the first half of the major shell and oblate shapes at the second half. In the present example with smaller quadrupole deformations the coupling is effective only inside the $\ell=4$ shell and the $\ell=7$ shell, respectively. Therefore, the obtained oblate-prolate preference in the self-consistent shape depending on the degree of the major-shell filling agrees with the feature of a single-ℓ-shell. An additional interesting feature of Fig. 19 is that the number of systems with prolate minimum is appreciably larger than that of oblate systems. Namely, for the system with particles half-filled in the major shell ($N=162$) the prolate shape is already much more favourable than the oblate shape. The competition between prolate and oblate shape shown in Fig. 19 could be sensitive to the accuracy in the calculation of the volume-conservation condition, in which we have not included the $\bar{\ell}^2$-term. Therefore, in Appendix B we have solved the problem of axially-symmetric quadrupole-deformation with an infinite square-well potential, taking precisely into account the volume-conservation. Our modified-oscillator potential is certainly different from the exact infinite-square-well potential and, thus, the details of the quantitative results coming from those two potentials are different. However, the answer to the question of which shape (oblate or prolate) is more favourable for a given particle-number is found to be very similar in Fig. 22 and in Fig. 19.

We note that only in the system with $152<N<158$ the energetically most favourable shape deviates considerably from axially-symmetric shape and, in fact, becomes $\gamma\sim 30°$. (For the definition of γ here, see Appendix 6B of [2]).

In Fig. 20 we show the plotting in Fig. 19 for a larger region of particle-numbers.

In Fig. 21 we plot Fig. 13 and Fig. 19 in the same frame. It is seen that for $152\leqq N\leqq 158$ the Y_{32}-deformation is clearly the most favourable deformation, although for $N<152$ the most favourable deformation is very close to the oblate one and for $N>158$ it is very close to the prolate one.

In order to discuss the equilibrium shapes of fermion systems one should consider quite general octupole deformations. Furthermore, one may not exclude the possibility that some combinations of octupole deformation together with quadrupole deformation could further lower the energy of the system. We will discuss this problem in a future publication.

5. Conclusions

Simulating the one-particle spectra of the infinite-well potential by those of a modified oscillator potential, we have investigated the possible occurrence of octupole (as well as quadrupole) deformations in systems with particle-number up till 200. For simplicity, and keeping in mind the fact that a possible immediate application of the result of the present investigation could be the system of metal clusters, we neglect the spin-orbit potential. Among various types of octupole deformations we have found that the Y_{32}-type deformation is especially interesting, because of the occurrence of highly-degenerate single-particle levels due to the T_d-group symmetry and because of the strong shell-structure (namely, the strong bunching) of the resulting one-particle spectra. It is interesting to observe that the axially-symmetric octupole deformation (i.e. Y_{30}-deformation) almost never wins in any particle-number system, in competition with other types of octupole deformations.

It is found that in the major shell of the spherical shape with $138 < N \leqq 186$, for example, the quadrupole-deformed almost-oblate shape is clearly most favourable for $146 \leqq N < 152$, while the nearly prolate shape is most favourable for $N > 158$. Exactly in the region of the particle-number ($152 \lesssim N \lesssim 158$) in which the quadrupole-deformed shape with a considerable amount of deviation from axial-symmetry wins against almost prolate or almost oblate deformations, the Y_{32}-deformation is found to be energetically far more favourable than these triaxial quadrupole deformations.

One of the authors (X.Z.Z.) would like to thank the Department of Mathematical Physics for the financial support as well as the hospitality extended to him, while the other (H.-X.X.) is grateful to Tord Bengtsson for teaching him how to use the computer plotting-programs.

Appendix A. Octupole deformations in terms of group theory

In this appendix we employ the notation for irreducible representations used in [4], and by the degree of degeneracy we mean that without the spin degree of freedom.

The Y_{30}-deformation is axially-symmetric. Namely, it has the symmetry of the D_∞ group. Thus, the angular-momentum component along the symmetry-axis, m, is a good quantum-number. The $m=0$ levels are singly-degenerate, while $m \neq 0$ levels are doubly-degenerate with $\pm|m|$.

The $(Y_{31} - Y_{3-1})$-deformation has the symmetry of the C_{2v}-group. The C_{2v}-group has four one-dimensional irreducible representations (see, for example, [4]). Thus, all levels are singly-degenerate.

The $(Y_{32} + Y_{3-2})$-deformation has the symmetry of the T_d-group, which has two one-dimensional (A_1 and A_2), one two-dimensional (E), and two three-dimensional irreducible representations (F_1 and F_2). In Table 1 we show the resolution of the $(2\ell+1)$-dimensional representation $D^{(\ell)}$ of the rotation group into the irreducible representations of T_d, together with the characters of the classes in $D^{(\ell)}$. For example, from the rows with $\ell=4$ and $\ell=7$ in Table 1 one obtains immediately the features of Fig. 2 for the Y_{32}-deformation. Namely, the irreducible representations of both one F_1 and one F_2 in $D^{(\ell=7)}$ have no partners in $D^{(\ell=4)}$. Both F_1 and F_2 are 3-dimensional and, thus, as a total 6 levels are not affected by the $(Y_{32} + Y_{3-2})$-coupling. The shifted levels are one singly-degenerate (A_1), one doubly-degenerate (E), and two triply-degenerate (F_1 and F_2), both upwards and downwards, symmetrically.

The $(Y_{33} - Y_{3-3})$-deformation has the symmetry of the D_{3h}-group, which has four one-dimensional (A_1', A_2', A_1'' and A_2'') and two two-dimensional irreducible representations (E' and E''). In Table 2 we show the resolution

Table 1. Resolution of $(2\ell+1)$-dimensional representation $D^{(\ell)}$ of rotation group into irreducible representations of T_d, together with characters of classes of T_d in $D^{(\ell)}$

Characters of classes of T_d in $D^{(\ell)}$						Resolution of $D^{(\ell)}$ into irreducible representation of T_d
ℓ	E	C_3	C_2	σ_d	S_4	
0	1	1	1	1	1	A_1
1	3	0	−1	1	−1	F_2
2	5	−1	1	1	−1	$E+F_2$
3	7	1	−1	1	1	$A_1+F_2+F_1$
4	9	0	1	1	1	$A_1+E+F_2+F_1$
5	11	−1	−1	1	−1	$E+2F_2+F_1$
6	13	1	1	1	−1	$A_1+A_2+E+2F_2+F_1$
7	15	0	−1	1	1	$A_1+E+2F_2+2F_1$

Table 2. Resolution of $(2\ell+1)$-dimensional representation $D^{(\ell)}$ of rotation group into irreducible representations of D_{3h}, together with characters of classes of D_{3h} in $D^{(\ell)}$

Characters of classes of D_{3h} in $D^{(\ell)}$							Resolution of $D^{(\ell)}$ into irreducible representation of D_{3h}
ℓ	E	σ_h	C_3	S_3	U_2	σ_v'	
0	1	1	1	1	1	1	A_1'
1	3	1	0	−2	−1	1	$A_2''+E'$
2	5	1	−1	1	1	1	$A_1'+E'+E''$
3	7	1	1	1	−1	1	$A_1'+A_2'+A_2''+E'+E''$
4	9	1	0	−2	1	1	$A_1'+A_1''+A_2''+2E'+E''$
5	11	1	−1	1	−1	1	$A_1'+A_2'+A_2''+2E'+2E''$
6	13	1	1	1	1	1	$2A_1'+A_2'+A_1''+A_2''+2E'+2E''$
7	15	1	0	−2	−1	1	$A_1'+A_2'+A_1''+2A_2''+3E'+2E''$

of the $(2\ell+1)$-dimensional representation $D^{(\ell)}$ of the rotation group into the irreducible representation of D_{3h}, together with the characters of the classes of D_{3h} in $D^{(\ell)}$. For example, from the rows with $\ell=4$ and $\ell=7$ in Table 2 we obtain the features of Fig. 2 for the Y_{33}-deformation. Namely, the irreducible representations of one A_2', one A_2'', one E' and one E'' in $D^{(\ell=7)}$ have no partners in $D^{(\ell=4)}$. Thus, as a total $6(=1+1+2+2)$ levels are not affected by the $(Y_{33}-Y_{3-3})$-coupling. The shifted levels are three singly-degenerate (A_1', A_1'' and A_2'') and three doubly-degenerate ($2E'$ and E''), both upwards and downwards, symmetrically.

Appendix B. One-particle motion in spheroidal box

In [6], S.A. Moszkowski studied the quantal spectrum of particle-motion in a spheroidal box by making an appropriate coordinate transformation so that the potential was brought to spherical symmetry. The effect of the non-spherical shape appeared then as a change in kinetic energy for which the non-spherical term can be diagonalized. In the transformed coordinates the boundary conditions require that the wave functions vanish at the radius of the sphere. In this formalism the volume-conservation condition can be easily taken into account in an exact way. Thus, it is instructive to calculate the quantities obtained in Sect. 4 so as to compare the results.

Using Moszkowski's method we solve the one-particle motion in the spheroidal (i.e. axially-symmetric quadrupole-deformed) box and calculate the same quantities as those shown in Fig. 19. The result is shown in Fig. 22. The details of the one-particle spectra in the infinite-well box are certainly different from those in our modified oscillator-potential, as is already seen in the comparison between Fig. 1 and Fig. 3 for a spherically-symmetric shape. (Moreover, in the comparison we note the difference between the used energy-unit in Fig. 1 and the one in Fig. 3). Consequently, we naturally expect some difference between Figs. 19 and 22. Here, we want to emphasize the two common characteristic features observed in both Figs. 19 and 22: Namely, (*a*) at the beginning of the major shell for spherical shape (with $138<N\leqq 186$) the oblate shapes are favourable while on the second half of the shell the prolate shapes are favourble; (*b*) the number of systems in which the prolate shape is more favourable than the oblate shape is larger than the number for which the oblate shape is more favourble.

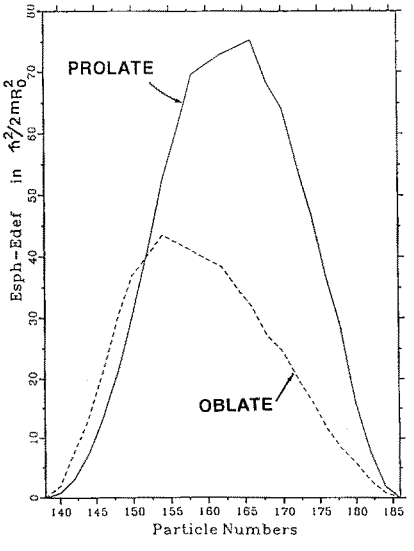

Fig. 22. The same quantity as Fig. 19, but calculated for the exact infinite-well axially-symmetric quadrupole-deformed potential (and not for our modified oscillator potential). The solid line corresponds to prolate shape, while the dashed line to oblate shape. Note the difference between the used energy-unit in Fig. 19 and in the present figure

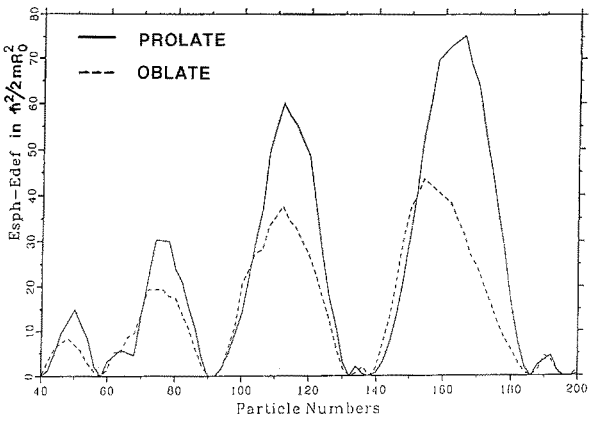

Fig. 23. The same quantity as Fig. 22 but for a larger region of the particle-number

In Fig. 23 we show the calculated results which may be compared with those shown in Fig. 20.

Appendix C. One-particle spectra for octupole-deformed potential in limit of large angular-momentum

In the limit of very large angular-momentum, ℓ, it is possible to obtain a simple analytic solution of the spectrum resulting from a degenerate pair of orbits ℓ and $\ell+3$ moving in an octupole potential. A similar approach has previously been employed in the analysis of single particle motion in rotating potentials [7] and the rotational motion of centrifugally distorted molecules [8]. This semiclassical solution can be exhibited most directly by taking the $\ell\gg 1$ limit of the octupole matrix-elements

$$\langle \ell+3, m+\mu | Y_{3\mu} | \ell, m\rangle = \sqrt{\frac{4\pi}{7}} \begin{pmatrix} \ell & 3 & \ell+3 \\ 0 & 0 & 0 \end{pmatrix} \begin{pmatrix} \ell & 3 & l+3 \\ m & \mu & -(m+\mu) \end{pmatrix}$$

$$= \text{const} \sqrt{\frac{6!}{(3+\mu)!\,(3-\mu)!} \frac{(\ell+3+\mu+m)!\,(\ell+3-\mu-m)!}{(\ell+m)!\,(\ell-m)!}}$$

$$\sim \sqrt{\frac{6!}{(3+\mu)!\,(3-\mu)!}} (\ell+m)^{3+\mu} (\ell-m)^{3-\mu}. \qquad \text{(C.1)}$$

We begin by considering the axially symmetric case, $\mu=0$. In this case the octupole potential only couples the states, $|\ell, m\rangle$ and $|\ell+3, m\rangle$. We describe this two-valued intrinsic variable by introducing the 2×2 Pauli matrices (τ_x, τ_y, τ_z) and associate the states $|\ell, m\rangle$ with $\tau_z=+1$ and $|\ell+3, m\rangle$ with $\tau_z=-1$. From (C.1) we then obtain the Hamiltonian matrix

$$h=\sqrt{20}(\ell^2-m^2)^{3/2}\tau_x \tag{C.2}$$

which is trivially diagonalized to obtain the eigenvalues

$$\varepsilon_0(m)=\pm\sqrt{20}(\ell^2-m^2)^{3/2}, \quad m=0, \pm 1, \pm 2, \ldots, \pm\ell. \tag{C.3}$$

The lowest and highest state has $m=0$ and is non-degenerate, while the $m\neq 0$ states are 2-fold degenerate. Especially for the $\mu\neq 0$ spectra to be discussed below it is convenient to view the spectrum (C.3) as representing the quantized results of classical motion of an angular momentum vector $\vec{\ell}$; since $|\vec{\ell}|=$constant the motion takes place on the surface of the sphere, $\ell_x^2+\ell_y^2+\ell_z^2=\ell^2$. The characterization of the motion can be based on the analysis of stationary points, where $\frac{d\vec{\ell}}{dt}=0$. The spectrum in the neighbourhood of stationary points is expressed by a small amplitude oscillation around those points and is analyzed by using semiclassical quantization.

In the following we discuss the stationary points in Sect. C. 1, while in Sect. C. 2 we describe small amplitude oscillations around the stationary points and the coupling due to tunneling effect.

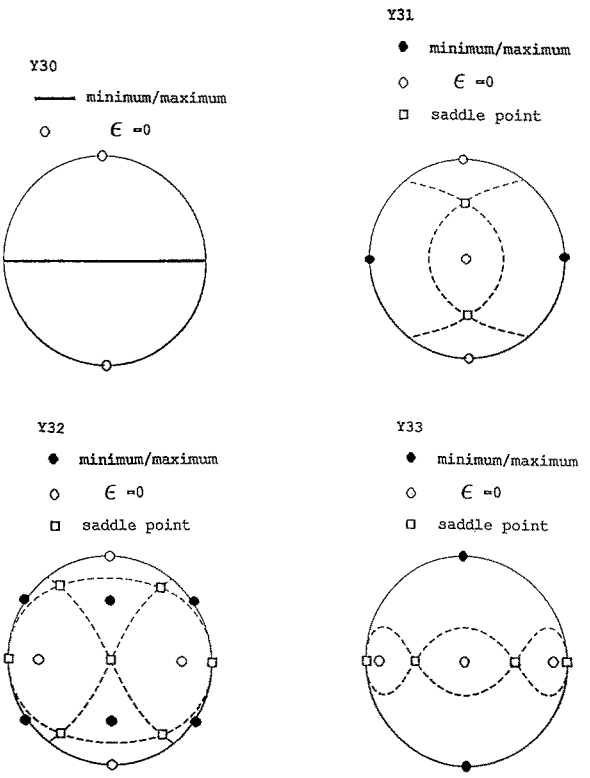

Fig. 24. Stationary points and separatrices of the reduced Hamiltonians, h_0 in (C.5) for the Y_{30} deformation, h_1 in (C.8) for the Y_{31} deformation, h_2 in (C.10) for the Y_{32} deformation, and h_3 in (C.12) for the Y_{33} deformation. The separatrices are denoted by dashed lines. The figure is drawn as seen from the positive x-axis and projected on the $y-z$ plane

C.1. Stationary points and separatrix

Introducing spherical coordinates

$$\begin{aligned}\ell_x&=\ell\sin\theta\cos\varphi,\\ \ell_y&=\ell\sin\theta\sin\varphi,\\ \ell_z&=\ell\cos\theta,\end{aligned} \tag{C.4}$$

the Hamiltonian associated with (C.3) is written as

$$h_0=\pm\sqrt{20}\,\ell^3\sin^3\theta. \tag{C.5}$$

We note that the eigenvalues in the present problem are always distributed symmetrically with negative and positive sign. The classical orbits on the sphere associated with (C.5) have the simple structure drawn in Fig. 24. The points denoted by open circles express the orbits with the zero-energy (i.e. $\varepsilon=0$), which are 2-fold degenerate, while the equator is the "minimum/maximum" energy. (The word, "minimum/maximum", means the minimum for the negative sign and the maximum for the positive sign in (C.5).) In the terminology of the group theory the Y_{30} potential has the symmetry of the D_∞-group and, due to the present approximation (i.e. $\ell\gg 1$), the Hamiltonian (C.5) has the symmetry of the $D_\infty\cdot C_i=D_{\infty h}$ group.

For $\mu=\pm 1$ we consider the effect of a real potential

$$V_1=\frac{1}{\sqrt{2}}(Y_{31}-Y_{3-1}), \tag{C.6}$$

which leads by means of (C.1) to the Hamiltonian

$$h=\sqrt{30}\,\ell^3\sin^2\theta(\cos\theta\cos\varphi\,\tau_x+\sin\varphi\,\tau_y). \tag{C.7}$$

Since the square of the h in (C.7) is independent of the τ-variables, we obtain the reduced Hamiltonian for the motion of $\vec{\ell}$,

$$h_1=\pm\sqrt{30}\,\ell^3\sin^2\theta\sqrt{\cos^2\theta\cos^2\varphi+\sin^2\varphi}. \tag{C.8}$$

The structure of the classical orbits associated with (C.8) is sketched in Fig. 24. There are 2 minimum/maximum points ($\theta=\pi/2$, $\varphi=\pm\pi/2$: $\varepsilon=\pm\ell^3\sqrt{30}$), 4 points with $\varepsilon=0$ ($\theta=0$; $\theta=\pi$; $\theta=\pi/2$, $\varphi=0$ and π), and 4 saddle points ($\theta=\cos^{-1}(\pm 1/\sqrt{3})$, $\varphi=0$ and π: $\varepsilon=\pm\ell^3\sqrt{40/9}$). Notice that the two $\varepsilon=0$ equatorial points are not equivalent to the other two $\varepsilon=0$ points (polar) as revealed for example by the small amplitude solutions discussed in Sect. C. 2. The classical orbits passing through the saddle points are the separatrices which divide the surface of the sphere into six regions. The Y_{31} potential in (C.6) has the symmetry of the C_{2v} group, while the reduced

Hamiltonian (C.8) has the symmetry of the $C_{2v}\cdot C_i = D_{2h}$ group.

For $\mu = \pm 2$ we consider a real potential

$$V_2 = \frac{1}{\sqrt{2}}(Y_{32} + Y_{3-2}), \tag{C.9}$$

which leads to the reduced Hamiltonian

$$h_2 = \pm\sqrt{12}\,\ell^3 \sin\theta[(1+\cos^2\theta)^2\cos^2(2\varphi) + 4\cos^2\theta\sin^2(2\varphi)]^{1/2}. \tag{C.10}$$

The structure of the classical orbits associated with (C.10) is sketched in Fig. 24. There are 8 minimum/maximum points ($\theta = \cos^{-1}(\pm 1/\sqrt{3})$, $\varphi = 0$, $\pi/2$, π and $3\pi/2$: $\varepsilon = \pm\ell^3\sqrt{128/9}$), 6 points with $\varepsilon = 0$($\theta = 0$; $\theta = \pi$; $\theta = \pi/2$, $\varphi = \pi/4$, $3\pi/4$, $5\pi/4$ and $7\pi/4$) and 12 saddle points ($\theta = \pi/2$, $\varphi = 0$, $\pi/2$, π, and $3\pi/2$; $\theta = \cos^{-1}(\pm 1/\sqrt{2})$, $\varphi = \pi/4$, $3\pi/4$, $5\pi/4$ and $7\pi/4$: $\varepsilon = \pm\ell^3\sqrt{12}$). The separatrices divide the surface of the sphere into 14 regions. The Y_{32} potential in (C.9) has the symmetry of the T_d group, while the reduced Hamiltonian (C.10) has the symmetry of the $T_d\cdot C_i = O_h$ group.

For $\mu = \pm 3$ we consider a real potential

$$V_3 = \frac{1}{\sqrt{2}}(Y_{33} - Y_{3-3}). \tag{C.11}$$

Then, the reduced Hamiltonian is obtained as

$$h_3 = \pm\sqrt{2}\,\ell^3[(1+3\cos^2\theta)^2\sin^2(3\varphi) + \cos^2\theta(3+\cos^2\theta)^2\cos^2(3\varphi)]^{1/2}. \tag{C.12}$$

In Fig. 24 we sketch the structure of the classical orbits associated with (C.12). There are 2 minimum/maximum points ($\theta = 0$ and π: $\varepsilon = \pm\ell^3\sqrt{32}$), 6 points with $\varepsilon = 0$($\theta = \pi/2$; $\varphi = 0$, $\pi/3$, $2\pi/3$, π, $4\pi/3$ and $5\pi/3$), and 6 saddle points ($\theta = \pi/2$; $\varphi = \pi/6$, $\pi/2$, $5\pi/6$, $7\pi/6$, $3\pi/2$ and $11\pi/6$: $\varepsilon = \pm\ell^3\sqrt{2}$). The separatrices divide the surface of the sphere into 8 regions. The Y_{33} potential in (C.11) has the symmetry of the D_{3h} group, while the reduced Hamiltonian (C.12) has the symmetry of the $D_{3h}\cdot C_i = D_{6h}$ group.

In Table 3 we summarize the result of the present Section C. 1.

Table 3. Symmetry of reduced Hamiltonian, (C.5), (C.8), (C.10) and (C.12), together with degeneracy and energy at stationary points

Hamiltonian	Symmetry	Minimum/Maximum		($\varepsilon = 0$) point	Saddle point	
		Degeneracy	Energy (in ℓ^3)	Degeneracy	Degeneracy	Energy (in ℓ^3)
h_0	$D_{\infty h}$	∞	$\pm\sqrt{20}$	2		
h_1	D_{2h}	2	$\pm\sqrt{30}$	4	4	$\pm\sqrt{40/9}$
h_2	O_h	8	$\pm\sqrt{128/9}$	6	12	$\pm\sqrt{12}$
h_3	D_{6h}	2	$\pm\sqrt{32}$	6	6	$\pm\sqrt{2}$

Table 4. Degeneracy and spectrum of small-amplitude harmonic oscillations around stationary points

Hamiltonian	Minimum/Maximum		($\varepsilon = 0$) point	
	Degeneracy	Spectrum (in ℓ^3)	Degeneracy	Spectrum (in ℓ^3)
h_0		0		0
h_1	2	$(n+\frac{1}{2})\sqrt{60}(1/\ell)$	2	$(n+\frac{1}{2})\sqrt{120}(1/\ell)$
			2	$\sqrt{(n+\frac{1}{2})}\sqrt{60}(1/\sqrt{\ell})$
h_2	8	$(n+\frac{1}{2})\sqrt{32}(1/\ell)$	6	$\sqrt{(n+\frac{1}{2})}\sqrt{96}(1/\sqrt{\ell})$
h_3	2	$(n+\frac{1}{2})\sqrt{72}(1/\ell)$	6	$\sqrt{(n+\frac{1}{2})}\sqrt{36}(1/\ell)$

C.2. Small-amplitude oscillations around stationary points and coupling due to tunneling effect

The orbits in the neighbourhood of the minimum/maximum points as well as the $\varepsilon = 0$ points can be analyzed by expanding the reduced Hamiltonian at those points to the second order of canonical variables (a harmonic approximation), (p, q), and, then, by employing the semiclassical quantization condition

$$\oint p\,\mathrm{d}q = 2\pi\hbar(n+\tfrac{1}{2}), \tag{C.13}$$

where $n = 0, 1, 2, \ldots$. We have found two different kinds of the second-order Hamiltonian, depending on cases. Namely, either the form

$$h' = ap^2 + bq^2, \tag{C.14}$$

or the form

$$h' = \sqrt{ap^2 + bq^2}. \tag{C.15}$$

The Hamiltonian in (C.14) leads to the quantized spectra $\varepsilon_n = (n+1/2)\hbar\omega$, while the one in (C.15) produces the spectra $\varepsilon_n = \sqrt{n+1/2}\hbar\omega$.

In Table 4 the calculated results are given. For example, in the case of h_1 (i.e. the Y_{31}-deformation) the tabulated small-amplitude harmonic oscillations around the $\varepsilon = 0$ points contain both of the above two kinds of spectra. Namely, for the 2 points with $\varepsilon = 0$ (i.e. $\theta = 0$ and $\theta = \pi$) the second-order Hamiltonian has the form of (C.14) and, thus, the spectrum is $\varepsilon_n = (n+1/2)\sqrt{120}(1/\ell)$. In contrast, for the 2 points with $\varepsilon = 0$ (i.e. $\theta = \pi/2$, $\varphi = 0$ and π) the Hamiltonian h' has the form of (C.15) and leads to the spectrum $\varepsilon_n = \sqrt{n+1/2}\sqrt{60}(1/\sqrt{\ell})$.

Using quantum-mechanical bases, $|\ell, m\rangle$ and $|\ell+3, m\rangle$, for $\ell \approx 70$, we have performed exact numerical diagonalization of the Hamiltonian, (C.2), (C.7) and so on. Then, with remarkable accuracy we have confirmed both the degeneracies and the structure of the spectra, corresponding to Table 4.

Now, in the calculation of the results given in Tables 3 and 4 the coupling through the quantum-mechanical tunneling between the equivalent stationary points was neglected. When this coupling is included, the levels which are degenerate in the tables may exhibit a fine

structure of the splitting. The splitting may be observed in the actual physical system such as metal clusters or molecules, in which the relevant angular-momentum could be large but finite. The essence of the calculation of the splitting has already been worked out in [8]. Therefore, in the following we briefly illustrate the fine structure, by taking as an example the 8-fold degeneracy at the minimum/maximum points of the Hamiltonian h_2.

Taking the axis which goes through the origin as well as one of the 8 minimum/maximum points in Fig. 24, we see that it is an axis of symmetry of the third order. (It is trivial that taking any one of those 8 points leads to the equivalent result.) In other words, it has the symmetry of the C_3 group. Taking the axis as a quantization axis and expressing the component of $\vec{\ell}$ along the axis by m, a given irreducible representation (IR) of C_3 contains only the m-values which satisfy the condition

$$m \equiv i \quad \text{MOD } 3, \tag{C.16}$$

with a given i-value. The values of i can be 0 or 1 or 2. Each 8-dimensional representation of the T_d group corresponds to a particular IR of the C_3 group, which can be resolved into the IR of the T_d group as follows.

$$\begin{aligned} &i=0;\ A_1+F_1+F_2+A_2 \\ &i=1;\ F_1+E+F_2 \\ &i=2;\ F_1+E+F_2 \end{aligned} \tag{C.17}$$

where we have used the notation of IR in [4], as was done previously. Transforming the reduced Hamiltonian h_2 in (C.10) into the coordinate system with the present quantization axis, it is seen that $m=\ell$ is one of the 8 minimum/maximum points. That means, the resolution (C.17) can be written as

$$\begin{aligned} &(1)\ A_1+F_1+F_2+A_2 \quad \text{for } \ell \equiv 0 \text{ MOD } 3 \\ &(2)\ F_1+E+F_2 \quad \text{for } \ell \equiv 1 \text{ MOD } 3 \\ &(3)\ F_1+E+F_2 \quad \text{for } \ell \equiv 2 \text{ MOD } 3. \end{aligned} \tag{C.18}$$

In order to estimate, in the lowest-order approximation, the splitting of a given 8-dimensional cluster with a given value of $\ell \equiv i$ MOD 3 in (C.18), we note that each of 8 minimum/maximum points has 3 nearest neighbours. For example, the minimum/maximum point at ($\theta = \cos^{-1}(1/\sqrt{3})$, $\varphi=0$) in Fig. 24 has the 3 nearest neighbours at ($\theta=\cos^{-1}(-1/\sqrt{3})$, $\varphi=0$), ($\theta=\cos^{-1}(1/\sqrt{3})$, $\varphi=\pi/2$) and ($\theta=\cos^{-1}(1/\sqrt{3})$, $\varphi=3\pi/2$). Denoting the coupling (due to the tunneling effect) to those nearest neighbours by S, one obtains the energy splitting as follows.

$$\begin{aligned} &(1)\ A_1:\ 3S, F_1:\ S, F_2:\ -S, \quad A_2:\ -3S, \\ &\qquad\qquad\qquad\qquad\qquad \text{for } \ell \equiv 0 \text{ MOD } 3 \\ &(2) F_2:\ 2S, E:\ 0, F_1:\ -2S, \quad \text{for } \ell \equiv 1 \text{ MOD } 3 \\ &(3) F_2:\ 2S, E:\ 0, F_1:\ -2S, \quad \text{for } \ell \equiv 2 \text{ MOD } 3. \end{aligned} \tag{C.19}$$

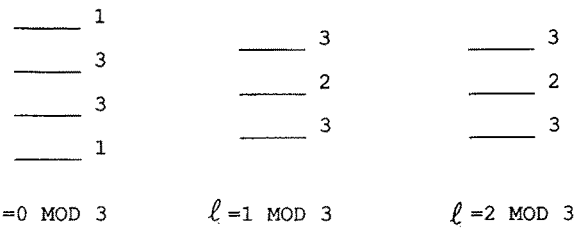

Fig. 25. Qualitative sketch of estimated splitting of 8 minimum/maximum points in the reduced Hamiltonian h_2 in (C.10) due to tunneling effect, depending on ℓ-values. The degrees of the degeneracy of resulting levels are given besides each line

In Fig. 25 we illustrate the obtained fine structure of the splitting of the 8 minimum/maximum points in the reduced Hamiltonian h_2. In order to obtain a very quantitative result of the splitting, one has to take into account the non-orthogonality of used bases described as "neighbours", the couplings to the next nearest neighbours, and so on. (See [8], for example.) However, performing an exact quantum-mechanical diagonalization with $\ell \approx 70$, we have confirmed the qualitative feature of the splitting (together with the degeneracy), which is exhibited in Fig. 25.

When we transform the reduced Hamiltonian (C.10) into the coordinate system defined in the last paragraph, in the neighbourhood of the minimum/maximum points with $m=\ell$ the Hamiltonian can be written as

$$h_2 = \pm \ell^3 \sqrt{128/9} \mp \ell^3 \sqrt{32}\left(1-\frac{m}{\ell}\right). \tag{C.20}$$

The spectrum (C.20) is in agreement with the result, which is tabulated in Tables 3 and 4 and which is obtained from the semiclassical quantization. Namely, around the minimum/maximum point the angular-momentum $\vec{\ell}$ performs a harmonic oscillation in a plane perpendicular to the z-axis and, thus, $m=\ell_z$ is a constant of motion.

References

1. Hamamoto, I., Mottelson, B.: Nucl. Phys. A**507**, 65c (1990)
2. Bohr, A., Mottelson, B.R.: Nuclear Structure, Vol. 2, New York: Benjamin Cummings, 1975
3. Heer, W.A. de, Knight, W.D., Chou, M.Y., Cohen, M.L.: Solid State Physics **40**, 93 (1987)
4. Landau, L.D., Lifshitz, E.M.: Quantum Mechanics, Chap. XII, 2nd Edn. Oxford: Pergamon Press
5. Nilsson, S.G.: K. Dan. Vidensk. Selsk. Mat. Fys. Medd. **29** (1955) No. 16
6. Moszkowski, S.A.: Phys. Rev. **99**, 803 (1955)
7. Bohr, A., Mottelson, B.R.: Phys. Scr. **22**, 461 (1980)
8. Harter, W.G., Patterson, C.W.: J. Chem. Phys. **66**, 4872 (1977); Patterson, C.W., Harter, W.G.: J. Chem. Phys. **66**, 4886 (1977)